# System Identification and Beam Current Control of a Radio-Frequency Ion Thruster Applied to Different Types of Coil Geometry

## IEPC-2017-331

*Presented at the 35th International Electric Propulsion Conference*
*Georgia Institute of Technology – Atlanta, Georgia – USA*
*October 8–12, 2017*

Niklas Wolf*
*University of Giessen, Giessen, 35392, Germany*
*Technische Hochschule Mittelhessen University of Applied Sciences, Giessen, 35390, Germany*

Peter J. Klar†
*University of Giessen, Giessen, 35392, Germany*

*and*

U. Probst‡
*Technische Hochschule Mittelhessen University of Applied Sciences, Giessen, 35390, Germany*

**Abstract: In this work we present an analysis of a radio-frequency ion thruster (RIT) regarding its dynamic behavior using the computed thruster's transfer function. Based on this analysis, the beam current controller (BCC) is designed.**

**System dynamics are analyzed using system identification algorithms. For this purpose, small changes are applied to input parameters of the thruster while observing the resulting beam current. The measured data can then be converted into a transfer function which represents the dynamic system behavior at the particular operating point. For a couple of operating points, these measurements are carried out repeatedly. Yielding a parameter set that can be used to design the BCC.**

**First, the functional principle of a RIT and the structure of the test setup are explained. Then the process of identification is described and results are presented for two coil geometries at different operating frequencies. Finally, the controller design is carried out, whose simulated control behavior is verified experimentally.**

*Research Assistant, Department of Electrical Engineering, niklas.wolf@ei.thm.de
†Professor, Institute of Experimental Physics I, peter.j.klar@exp1.physik.uni-giessen.de
‡Professor, Department of Electrical Engineering, uwe.probst@ei.thm.de

## Nomenclature

| | |
|---|---|
| BCC | = beam current control(ler) |
| $e$ | = elementary charge |
| $F$ | = thrust |
| $G_0$; $G_{\mathrm{I_{B,ref}}}$ | = transfer function of the open and closed control loop |
| $G_{\mathrm{uib}}$; $G_{\mathrm{mfib}}$; $G_{\mathrm{a}}$ | = transfer functions of the RIT-describing system model |
| $G_{\mathrm{R}}$ | = transfer function of the controller |
| $I_{\mathrm{acc}}$ | = current to acceleration grid |
| $I_{\mathrm{B}}$ | = ion beam current |
| $I_{\mathrm{B,mf}}$; $I_{\mathrm{B,v}}$ | = outputs of the transfer functions (beam current) |
| $I_{\mathrm{dec}}$ | = current to deceleration grid |
| IOs | = short form of inputs and outputs |
| $I_{\mathrm{scr}}$ | = current from screen grid |
| $K_0$ | = gain of the open loop transfer function |
| $K_{\mathrm{p,uib}}$; $K_{\mathrm{p,mfib}}$; $K_{\mathrm{p,a}}$ | = gain of the transfer functions |
| $\dot{m}$ | = mass flow of proprellant (xenon) |
| MFC | = mass flow controller |
| $m_{\mathrm{i}}$ | = mass of singly ionized particles |
| NHV | = negative high voltage power supply |
| PHV | = positive high voltage power supply |
| PM | = performance mapping |
| PI | = controller with a proportional and integral element |
| $P_{\mathrm{rfg}}$ | = dc-power of the RFG |
| RFG | = radio-frequency generator |
| RIT | = radio-frequency ion thruster |
| RTMU | = real-time measurement unit |
| $T_{\mathrm{a}}$; $T_{\mathrm{dn}}$; $T_{\mathrm{mfib}}$; $T_{\mathrm{n}}$ | = time constants of the transfer functions |
| $T_{\mathrm{i}}$ | = time constant of the PI-controller |
| $V_{\mathrm{acc}}$ | = acceleration grid voltage |
| $V_{\mathrm{ex}}$ | = total potential between screen and acceleration grid |
| $V_{\mathrm{rfg,dc}}$ | = dc input voltage of the RFG |
| $V_{\mathrm{scr}}$ | = screen grid voltage |

# I. Introduction

ELECTRIC propulsion is a technology aimed at achieving thrust using electrical power by accelerating particles to high velocities by different electrical and/or magnetic means. Increasing the exhaust velocity of outgoing particles twentyfold compared to a classical chemical thruster, the use of electrical power immensely improves the performance. Accordingly, less propellant is required for the generation of the thrust, resulting in a higher mass efficiency. This work focuses on radio-frequency ion thrusters, in particular, the RIT.

In cooperation with the University of Giessen, the research group of the Technische Hochschule Mittelhessen in Giessen works on optimizing the radio-frequency ion thrusters' overall efficiency by developing simulation models describing the RF thrusters' impedance and performance[1,2] and the ion extraction[3] as well as analyzing electromagnetic compatability[4]. Another topic is the development of electronics such as the radio-frequency generator[5,6] or the high voltage power supplies[7] with focus on switching loss optimization and exploring novel approaches.

Ion thrusters exhibit the highest efficiency and very high specific impulse compared to other thruster types. However, a major disadvantage of gridded ion thrusters is the erosion of the grids as a result of inefficient ion optics which limits the lifetime of a RIT. Consequently, it is important to minimize erosion of the grids to maximize lifetime. To minimize the effects of erosion, an understanding of the static and dynamic behavior of the system must be obtained.

The knowledge of the system's dynamic behavior, determined with system identification, is helpful for designing the beam current controller (BCC). System identification and the BCC design are the main subjects of this work.

# II. RIT Principle of Operation

The generation of thrust in RITs can be divided into two steps: ionization and extraction. A schematic image of the operating principle is shown in Fig. 1.[9,10] As can be seen in the figure, the commonly used propellant is the noble gas xenon. The gaseous flow into the ionization chamber is controlled and limited by the MFC. The chamber is surrounded by a rf-coil into which a sinusoidal RF-current is fed. By means of the current, an axial magnetic field, and as a result, an azimuthal electric field are induced, the latter accelerates free electrons inside the gas inside the chamber. Due to impact ionization, a self-sustaining plasma-discharge takes place.

After ionizing the propellant, ions can be extracted by applying an electrostatic field to the extraction grids generating thrust, given by the following equation:

$$F = I_{\mathrm{B}}(V_{\mathrm{ex}}, P_{\mathrm{rfg}}, \dot{m}) \cdot \sqrt{\frac{2 \cdot m_{\mathrm{i}} \cdot V_{\mathrm{scr}}}{e}}\,. \tag{1}$$

As can be seen, thrust depends on the beam current $I_{\mathrm{B}}$, the atomic mass $m_{\mathrm{i}}$ of the ions, the elementary charge $e$, and the screen voltage $V_{\mathrm{scr}}$ at the plasma-sided grid. The beam current itself depends on the dc power fed into the RFG $P_{\mathrm{rfg}}$, the supplied mass flow of propellant $\dot{m}$, and the extraction voltage, i.e. the total potential difference between the first and the second grid, defined as follows:

$$V_{\mathrm{ex}} = V_{\mathrm{scr}} + |V_{\mathrm{acc}}|\,. \tag{2}$$

The beam current $I_{\mathrm{B}}$ is given by the total number of ions leaving the system ($I_{\mathrm{scr}}$) minus the current at the acceleration ($I_{\mathrm{acc}}$) and deceleration grid ($I_{\mathrm{dec}}$). $I_{\mathrm{acc}}$ and $I_{\mathrm{dec}}$ are produced through over- or under-perveance as well as charge-exchange currents and are to be avoided since they lead to grid erosion. All grid currents are measured and the resulting beam current is then calculated as follows:

$$I_{\mathrm{B}} = |I_{\mathrm{scr}} - I_{\mathrm{acc}} - I_{\mathrm{dec}}|\,. \tag{3}$$

# III. Test Setup

In order to test the RIT, a test setup was constructed, which is shown in Fig. 2. In addition to the RIT and the external devices, a current measurement and a low-pass filter for eliminating RF disturbances were added. Its most important part is the real-time measurement unit (RTMU), which is used for controlling and monitoring the external devices as well as for recording the relevant system quantities. Matlab and Simulink

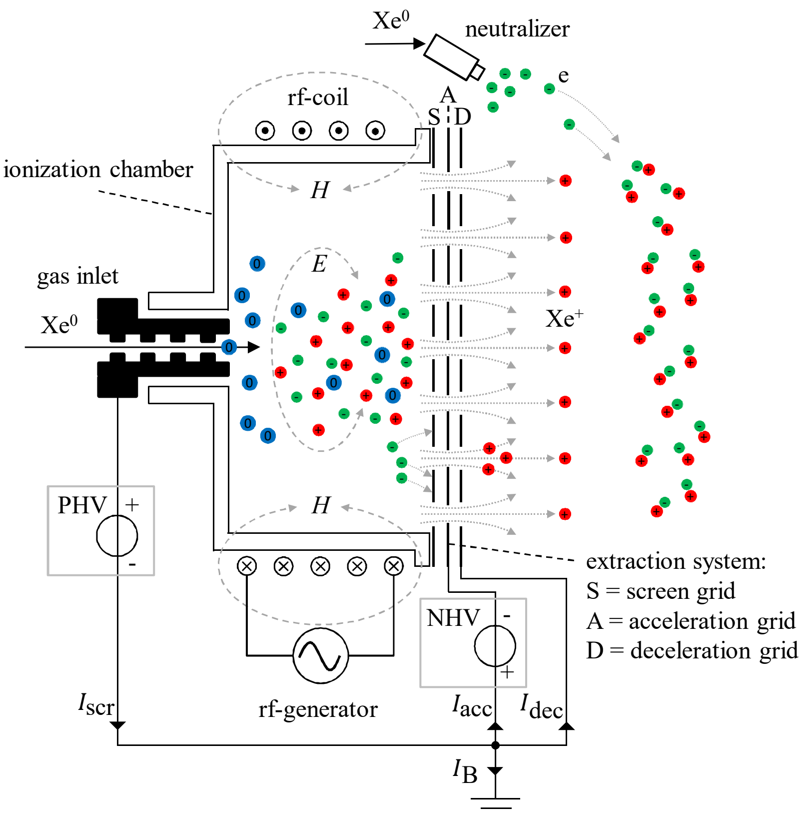


Figure 1: Function principle of a RIT.

are used for developing controller designs and to evaluate measured data. Analog and digital IOs as well as serial interfaces are used for communication purposes. In conjunction with so-called Matlab-scripts, data can be collected fully automatically.

A RIT wih 4 cm diameter (RIT4) is used. In order to verify the principle of system analysis based on system identification as well as on beam current control, the measurements are applied to two types of coil geometry, the conventional single-wound and a patent-pending bifilar coil geometry. The setups of both geometries are shown in Figure 3.

## IV. System Identification

System identification is used to evaluate the system's dynamic behavior. For this purpose, a mathematical model will be derived from experimental data, presenting the behavior of the system in terms of transfer functions. These experiments are based on assumptions regarding the model structure and the order of the transfer functions. Some results and a derived model have already been published in Ref. 8. In contrast to Ref. 8, in this work, a simplified model according to Fig. 4a is used. Only the mass flow $\dot{m}$ and the DC input voltage of the RFG $V_{\mathrm{rfg,dc}}$ are applied to the plant model as input parameters. The transfer function $G_{\mathrm{uib}}(s)$ describes the influence of the actuating variable $V_{\mathrm{rfg,dc}}$ on the system's output $I_{\mathrm{B,v}}$ representing the system's control transfer function, while changing the mass flow $\dot{m}$ corresponds to a disturbance the controller has to respond to. Therefore, $G_{\mathrm{mfib}}(s)$ is treated as the disturbance transfer function with the output $I_{\mathrm{B,mf}}$. The sum of both outputs is equal to the beam current. The RFGs DC voltage is used for the identification algorithms. Ideal signals are used for simulation and controller design, the power supply unit must be implemented into the simulation model as transfer function $G_{\mathrm{a}}(s)$, since otherwise erroneous dynamic behavior is simulated. The transfer function of the power supply $G_{\mathrm{a}}(s)$ as well as the disturbance

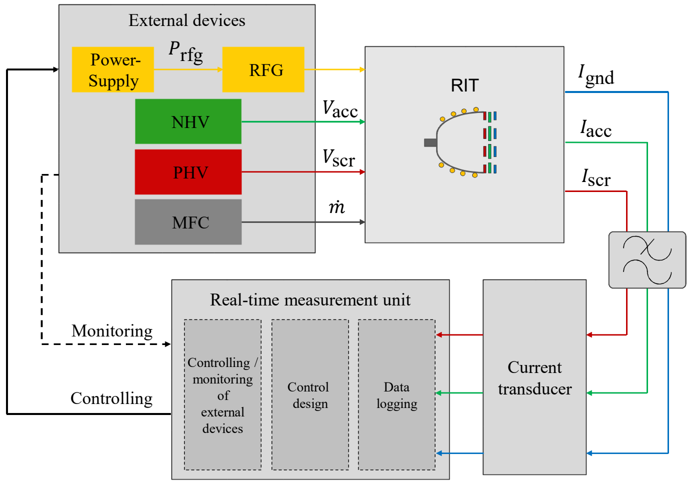


Figure 2: Schematic of the test setup for measurements at the RIT.

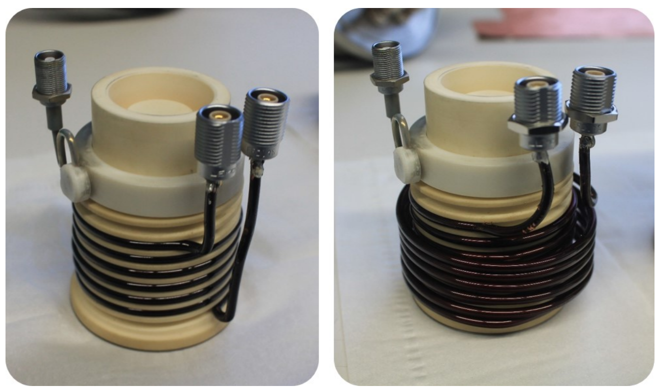

Figure 3: Conventional coil (left) and bifilar-wound coil (right).

transfer function $G_{\text{mfib}}(s)$ can be described as a first order delay $\text{PT}_1$, given by Eq. (4) and (5), respectively:

$$G_{\text{mfib}}(s) = G_{\text{PT}_1}(s) = K_{\text{p,mfib}} \cdot \frac{1}{1 + T_{\text{mfib}} \cdot s} \tag{4}$$

$$G_{\text{a}}(s) = G_{\text{PT}_1}(s) = K_{\text{p,a}} \cdot \frac{1}{1 + T_{\text{a}} \cdot s} \,. \tag{5}$$

Both are first order transfer functions with one pole and two parameters representing the gain $K_{\text{p}}$ and the time constant $T$. The transfer function of $G_{\text{uib}}(s)$ is also of first order, but includes one additional zero point. Equation (6) describes the transfer function of $G_{\text{uib}}(s)$:

$$G_{\text{uib}}(s) = K_{\text{p,uib}} \cdot \frac{1 + T_{\text{n}} \cdot s}{1 + T_{\text{dn}} \cdot s} \,. \tag{6}$$

Depending on the ratio of the time constants $T_{\text{n}}$ and $T_{\text{dn}}$, the transfer function $G_{\text{uib}}(s)$ results in a proportional ($\text{PPT}_1$) or differential ($\text{PDT}_1$) system behavior:

$$\frac{T_{\text{n}}}{T_{\text{dn}}} < 1 \rightarrow \text{PPT}_1 \tag{7}$$

$$\frac{T_{\text{n}}}{T_{\text{dn}}} > 1 \rightarrow \text{PDT}_1 \,. \tag{8}$$

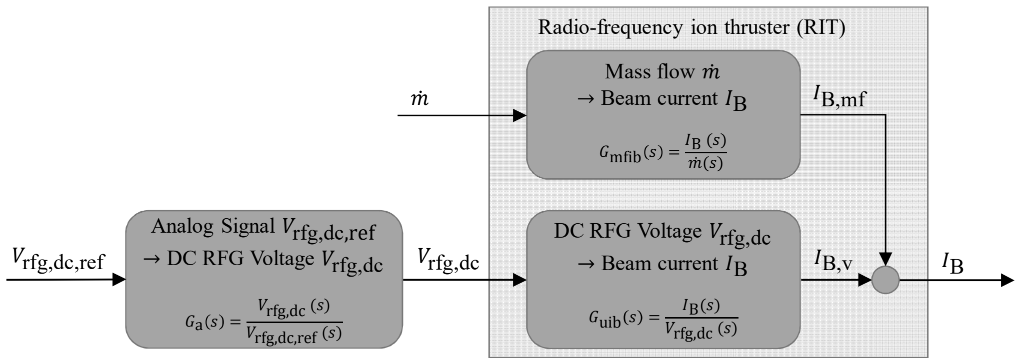


a)

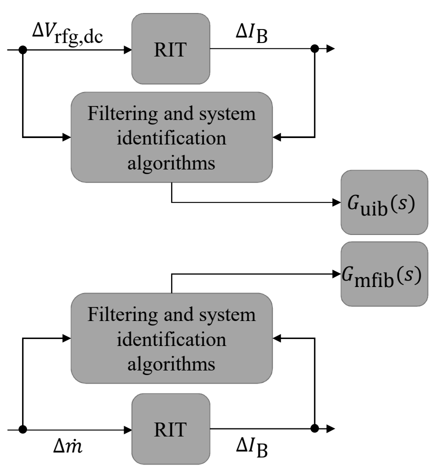


b)

Figure 4: a) Resulting system transfer functions of the RIT. b) Block diagram of the system identification process.

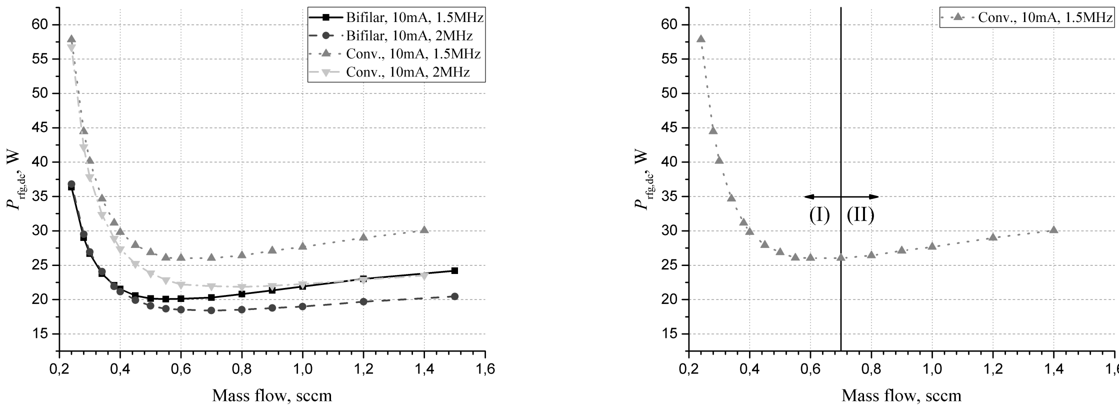


a) b)

Figure 5: a) Four measured performance mappings with a beam current of 10 mA at two different RF-frequencies (1.5 MHz and 2 MHz) of a conventional and of a bifilar-wound coil. b) Single PM for describing the two areas on the left (I) and right(II) of the minimum of required power.

Both, structure and number of parameters of the desired transfer function must be defined prior to the identification process. These considerations have been made in advance, see Reference 8. After defining the model structure, the identification process is executed as shown in Fig. 4b: According to simulation results[3], the grid voltages are set to a positive voltage of 900 V ($V_{\mathrm{scr}}$) and a negative voltage of $-50$ V ($V_{\mathrm{acc}}$), in order to minimize currents at the acceleration and deceleration grid. For a constant beam current of 10 mA, sixteen different values of mass flow are used for each PM, in the following called "operating points". In every single operating point, mass flow or RFG DC input voltage, respectively, will undergo small changes. The recorded input ($\Delta\dot{m}$ or $\Delta V_{\mathrm{rfg,dc}}$) to output ($\Delta I_{\mathrm{B}}$) data is filtered by a digital low-pass or band-stop filter and forwarded to the identification algorithm[13] which calculates the parameters of the transfer function, e.g. with the Gauss-Newton method. Filtering of the signal is required due to coupled RF disturbances in order to improve the identification. The so-called performance mapping (PM) is used for the selection of different operating points in which the transfer functions are identified. The PM is a characteristic curve which connects the DC power forwarded to the RFG with mass flow at fixed beam currents. Fig. 5a shows the measured Performance Mappings for both coil geometries and different RF-frequencies (1.5 MHz and 2 MHz) at a constant beam current of 10 mA. Applying the system identification to the PM data results in transfer functions as a function of the mass flow for a defined beam current (10 mA). Thus, a parameter set can be stored for each point located on the PM. For the transfer function $G_{\mathrm{a}}(s)$ of the actuator, the identification process is performed only once due to a nearly constant system behavior.

The results of the system identification for the transfer function $G_{\mathrm{uib}}(s)$ and $G_{\mathrm{mfib}}(s)$ are shown in Fig. 6 and Fig.7, respectively for the time constants $T_{\mathrm{n}}$, $T_{\mathrm{dn}}$ and $T_{\mathrm{mfib}}$, no clear trends are observed. With respect to the parameters, the PM can be divided into two different areas, shown in Fig. 5b. Each curve in the PM exhibits a minimum. The minimum is the mass flow at which a lowest power is required for the specified beam current. Area (I) describes the left-hand side of this point, i.e. low mass flow. The right side, towards higher mass flow, is defined as region (II). In (I), a strongly increased need of power is obtained to produce the same amount of beam current as the mass flow increases. Also on the right-hand side, in area (II), an increased need of power can be seen on increasing the mass flow, however with a markedly lower gradient. The fact that more power is required in these areas can be explained by a reduced conductivity of the plasma and its dependence of neutral gas density as discussed in Ref. 1,2 and 11.

For $G_{\mathrm{uib}}(s)$, shown in Fig. 6, only $K_{\mathrm{p,uib}}$, $T_{\mathrm{dn}}$ and the ratio of time constants $T_{\mathrm{n}}/T_{\mathrm{dn}}$ (logarithmic scale) are plotted. Taking a look at $T_{\mathrm{dn}}$, a trend cannot be recognized, however, a very well-matched system behavior can be achieved by setting the time constant in the range of some milliseconds. Considering the gain factor $K_{\mathrm{p,uib}}$ in (I), a higher voltage difference ($\mathrm{d}V$) is required for changing the beam current, which is equivalent to a decrease of the gain. At higher mass flows (II), a nearly linear increase of $K_{\mathrm{p,uib}}$ is obtained.

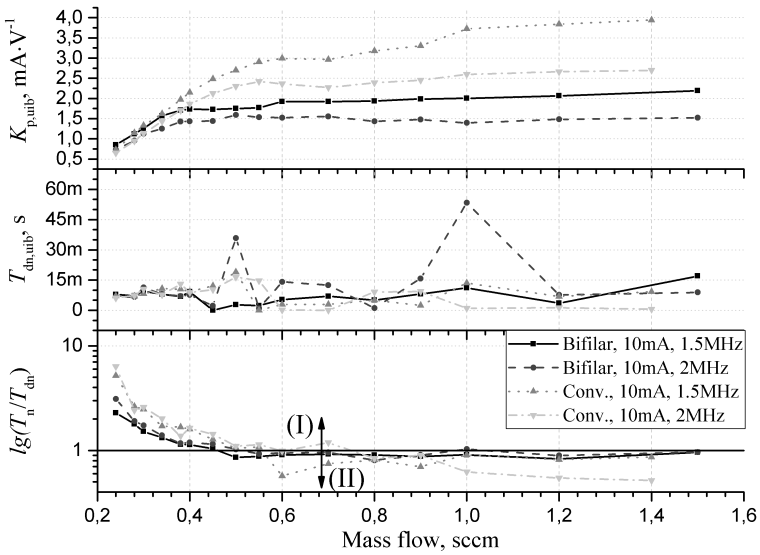


Figure 6: Parameters of the transfer function $G_{\rm uib}$. The ratio $T_{\rm n}/T_{\rm dn}$ is given in logarthmic scale.

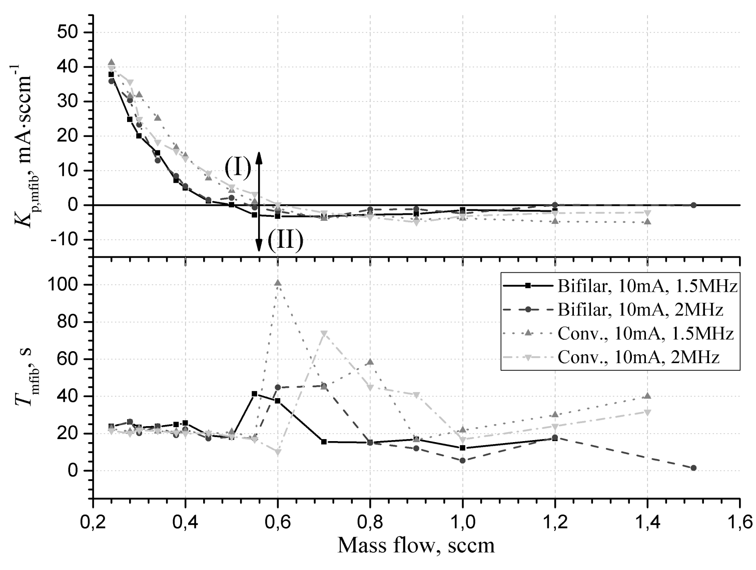


Figure 7: Parameters of the transfer function $G_{\rm mfib}$.

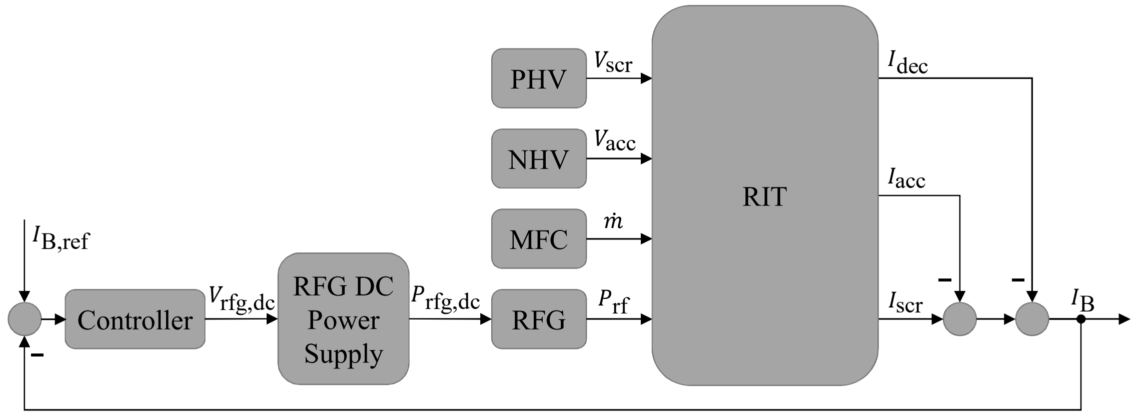


Figure 8: Schematic of the closed control loop with the DC RFG voltage as the actuator to manipulate the control variable $I_B$ given set by the reference $I_{B,ref}$.

Interesting is the ratio of the time constants, referring to the bottom plot in Fig. 6: higher mass flows result in an independence of $T_n/T_{dn}$ of mass flow and a pure proportional system behavior, meaning a ratio less or equal to one. In (I) $\lg(T_n/T_{dn})$ depends on the mass flow. The ratio of time constants is greater than one, resulting in a differential system behavior, which becomes even more dominant with decreasing mass flows. A differential behavior means an overshoot in the step response of the beam current. The larger the differential part, the higher the overshoot.

Taking a look at Fig. 7, the parameters of $G_{mfib}(s)$, i.e. the influence of the mass flow on the beam current shows similar trends than $G_{uib}(s)$. The gain increases from the minima of the PMs to small mass flows (I), meaning small changes in the mass flow produce strong changes in the beam current. Going to higher mass flows, the gain decreases, reaching zero at the minima of the PMs and becoming negative with increasing mass flow (II). As a result, a decreasing beam current is obtained for an increasing supply of proprellant in area (II) and vice-versa for region (I). The time constant $T_{mfib}$ is almost steady in the range of low mass flows (I) about 20 s. In the vicinity of the PM minima, a sudden increase in the time constant can be observed. This is also explained by the change of the algebraic sign of the gain. In the minima, the system's gain becomes zero, resulting in a time constant going to infinity. Moving to the right-hand side of the minimum, the time constant decreases to the previous value of 20 s, and then increases continously to higher values. With respect to a compensation of the disturbance (e.g. feedforward control), the change in the algebraic sign of the transfer function is of crucial importance, since a wrong sign leads to an amplification.

## V. Beam Current Control

The beam current is influenced most easily by the power fed into the plasma. This is best done by adjusting the RFG DC voltage in case of deviations or changes of the setpoint. From these considerations, the closed loop of Fig. 8 can be formed in order to control the beam current. In terms of the transfer functions already described, $G_a(s)$ represents the RFG DC Power Supply, $G_{uib}(s)$ the RFG plus RIT and $G_{mfib}(s)$ the MFC combined with RIT. For the controller design, the following requirements must be fulfilled:

a. steady-state accuracy

b. stability

c. robustness

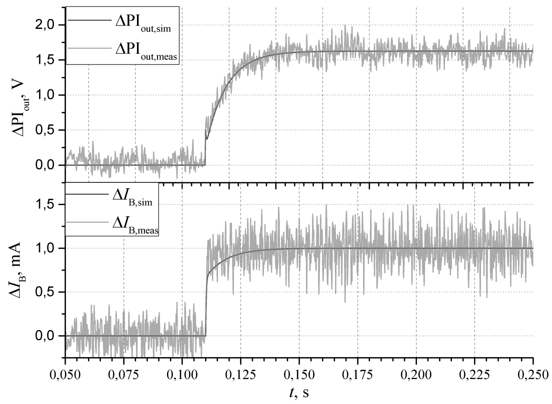


a) Conventional, $\dot{m} = 0.24$ sccm

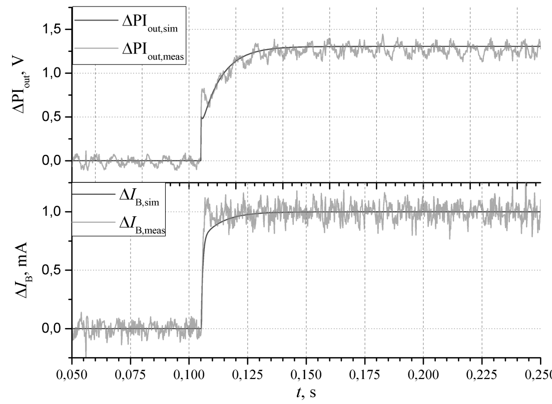


b) Bifilar, $\dot{m} = 0.24$ sccm

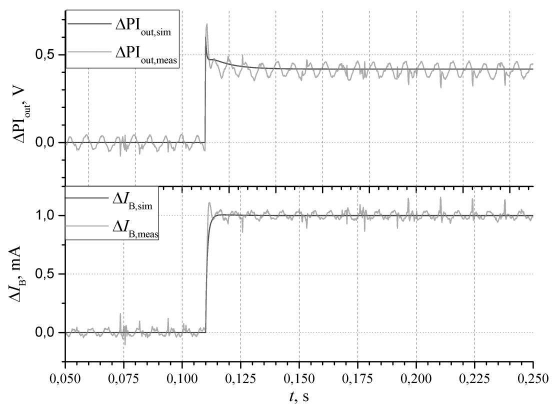


c) Conventional, $\dot{m} = 0.8$ sccm

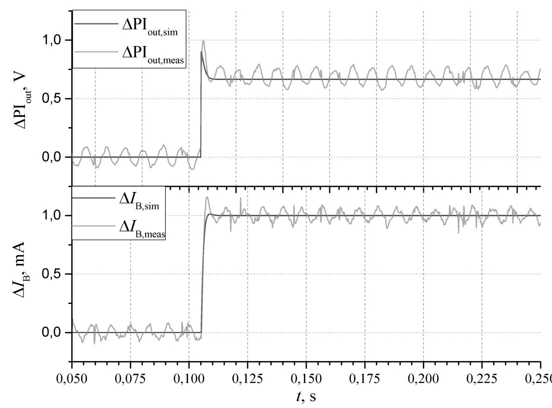


d) Bifilar, $\dot{m} = 0.8$ sccm

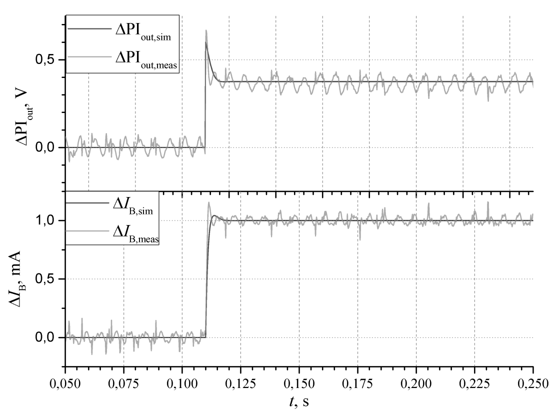


e) Conventional, $\dot{m} = 1.2$ sccm

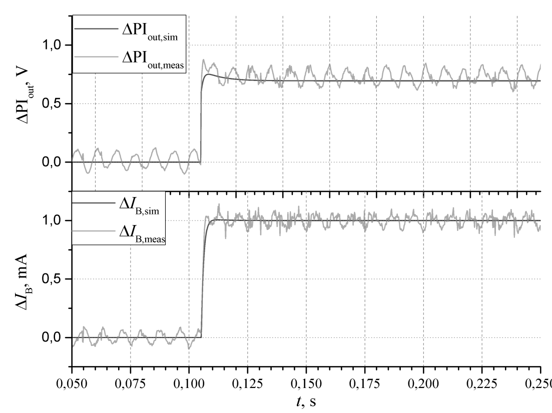


f) Bifilar, $\dot{m} = 1.2$ sccm

Figure 9: The output of the controller and the controlled beam current, simulated and measured for a normalized reference input of 9.5 mA to 10.5 mA for three different mass flows at 0.24 sccm, 0.8 sccm and 1.2 sccm. Both coil geometries were used with a beam current of 10 mA and a frequency of 2 MHz.

To accomplish requirement a, the control error must be zero in case of steady-state operation:

$$\lim_{t\to\infty}(I_{\mathrm{B,ref}}(t)-I_{\mathrm{B}}(t))=0\,.$$

In order to meet this condition, the open control loop must have integral behavior, resulting in a PI-controller with the following transfer function:

$$G_{\mathrm{R}}(s)=K_{\mathrm{R}}\cdot\frac{1+T_{\mathrm{i}}\cdot s}{T_{\mathrm{i}}\cdot s}\,. \tag{9}$$

Using $G_0(s)$ as the open loop transfer function, the transfer function $G_{\mathrm{I_{B,ref}}}(s)$ of the closed loop becomes:

$$\begin{aligned}G_0(s)&=G_{\mathrm{R}}(s)\cdot G_{\mathrm{a}}(s)\cdot G_{\mathrm{uib}}(s)\\&=\underbrace{K_{\mathrm{R}}\cdot K_{\mathrm{a}}\cdot K_{\mathrm{p,uib}}}_{K_0}\cdot\frac{1+(T_{\mathrm{i}}+T_{\mathrm{n}})\cdot s+T_{\mathrm{i}}\cdot T_{\mathrm{n}}\cdot s^2}{T_{\mathrm{i}}\cdot s\cdot(1+(T_{\mathrm{a}}+T_{\mathrm{dn}})\cdot s+T_{\mathrm{a}}\cdot T_{\mathrm{dn}}\cdot s^2)}\end{aligned} \tag{10}$$

$$\downarrow$$

$$G_{\mathrm{I_{B,ref}}}(s)=\frac{I_{\mathrm{B}}(s)}{I_{\mathrm{B,ref}}(s)}=\frac{G_0(s)}{1+G_0(s)}\,. \tag{11}$$

The requirement for stability (b.) implies that a finite excitation of the reference value leads to a finite output signal. The characteristic polynomial $(1+G_0)$ of the closed control loop has only zeros with negative real part, resulting in a given stability in all operating points[12]. Thus, for the controller design, no restriction in the selection of the control parameters $K_{\mathrm{R}}$ and $T_{\mathrm{i}}$ is given. For the investigations discussed in the following, a value of $K_{\mathrm{R}}=0.5$ was selected as control gain. The integral time is used to shorten the pole of the actuators transfer function $G_{\mathrm{a}}(s)$, which corresponds to the equilibrium of $T_{\mathrm{i}}$ with $T_{\mathrm{a}}$.

From the fact that a. and b. are met, it follows that c. is also fullfilled. The controller settings used, work for all operating points, while observing the required criteria.

That the statements are true is shown in Figure 9. It shows the change of the controller's output $\Delta\mathrm{PI_{out}}$ and the resulting controlled beam current $\Delta I_{\mathrm{B}}$, simulated and measured for a normalized reference input of $\Delta I_{\mathrm{B,ref}}=1$ mA for three different mass flows (0.24 sccm, 0.8 sccm and 1.2 sccm). The investigations were made for both coil geometries. It can be seen that the simulated and measured behavior agree well. Minor deviations can be explained by using a very high step function of the reference input (1 mA). The simulations show that the identified system behavior can be used for controller design. On the basis of the corresponding measurements, it can also be seen that the requirements for robustness, stability and good command response are fullfilled.

## VI. Conclusion and Outlook

In this paper, we have presented the possibility to describe the dynamic behavior of a radio-frequency ion thruster using transfer functions. These can in turn be used for controller design. The response of the system to a change in the reference variable was simulated and verified by measurements. Deviations in measured and simulated dynamic behavior/control behavior can result from the fact that, on one hand, a very large change in the size of the reference has been chosen and, on the other hand, effects such as thermodynamics have not yet been investigated. A further point to be investigated is the influence of the extraction voltages on the system. Thus "unfavorable" operating parameters still have to be examined, as in the case of defocusing, for example. The stability of the controller must also be ensured there.

From the point of view of control engineering, a general result of our investigation is, that the thruster is an easy-to-handle system. However, this applies only to the test setup used. If components of the system are replaced, e.g. another thruster is used, the dynamic properties also change and the investigations have to be repeated.

## References


[1]Volkmar, C., Ricklefs, U., and Klar, P. J., "Self-Consistent Numerical 0D/3D Hybrid Modeling of Radio-Frequency Ion Thrusters", *Transactions of the Japan Society for Aeronautical and Space Sciences*, Aerospace Technology Japan 14(ists30), pp. 23-32, 2016.

[2]Volkmar, C. and Ricklefs, U., "Implementation and Verification of a Hybrid Performance and Impedance Model of Gridded Radio-Frequency Ion Thrusters", European Physical Journal D 69(10), 227, 2015.

[3]Reeh, A., Probst, U., and Klar, P. J., "Numerical 3D Ion Extraction Code Incorporated Self-Consistency into a Model of a Radio-Frequency Ion Thruster", Proceedings of the 35th International Electric Propulsion Conference, Atlanta, Georgia, USA, 2017.

[4]Baruth, T., Thueringer, R., and Klar, P. J., "Radiated Emission Simulation of a RIT-4", Proceedings of the 34th International Electric Propulsion Conference, Kobe-Hyogo, Japan, Proc. IEPC-2015-411/ISTS-2015-b-411, 2015.

[5]Simon, J. and Probst, U., "High-Performance Digital-controlled Radio-Frequency Generator for RF Ion Thrusters", In Proceedings of the 6th Russian-German Conference on Electric Propulsion, Samara, Russia, 2016.

[6]Simon, J., Probst, U., and Klar, P. J., "Development of a Radio-Frequency Generator for RF Ion Thrusters", Proceedings of the 34th International Electric Propulsion Conference, Kobe-Hyogo, Japan, Proc. IEPC-2015-289/ISTS-2015-b-289, 2015.

[7]Roessler, C., Probst, U., and Simon, J., "Development of a Controlled High Voltage Power Supply for Gridded Ion Thrusters", Proceedings of the 35th International Electric Propulsion Conference, Atlanta, Georgia, USA, 2017.

[8]Wolf, N., Probst, U., and Klar, P. J., "System Identification of a Radio-Frequency Ion Thruster", Proceedings of the 34th International Electric Propulsion Conference, Kobe-Hyogo, Japan, Proc. IEPC-2015-292/ISTS-2015-b-292, 2015.

[9]Goebel, D. M., and Katz, I., *Fundamentals of Electric Propulsion*, John Wiley & Sons, Hoboken, 2008, Chap. 2.

[10]Leiter, H. J., Killinger, R., Bassner, H., Müller, J., Kukies, R., and Fröhlich, T, "Development and performance of the advanced radio frequency ion thruster RIT-XT", Proceedings of the 28th International Electric Propulsion Conference, ERPS, USA, 2003.

[11]Chabert, P., and Braithwaite, N., *Physics of Radio-Frequency Plasmas*, Cambridge University Press, Cambridge, 2011.

[12]Lunze, J., *Regelungstechnik 1*, Springer-Verlag, Berlin, 2010.

[13]Isermann, R. and Muenchhof, M., *Identification of Dynamic Systems*, Springer-Verlag, Berlin, 2011.